Flexible free-standing defect-rich MoS_2/graphene/carbon nanotube hybrid paper as binder-free anode for high-performance lithium ion batteries

Longsheng Zhang, Wei Fan and Tianxi Liu*

Electronic Supplementary Information

Fig. S1 FESEM image of bulk MoS_2.

Fig. S2 (a) FESEM, (b) TEM and (c, d) HRTEM images of df-MoS_2 NSs.

Fig. S3 (a) AFM images and (b) the corresponding height profiles of GO sheets.

Fig. S4 Cross-sectional FESEM images of (a) GC, (b) dr-MGC12, (c) dr-MGC11 and (d) dr-MGC21 hybrid papers.

Fig. S5 Cross-sectional FESEM images, corresponding EDS spectra and mapping images of (a) dr-MGC12, (b) dr-MGC11 and (c) dr-MGC21 hybrid papers.

Fig. S6 (a) Top-view and (b) cross-sectional FESEM images of dr-MG21 hybrid paper.

Fig. S7 Nitrogen adsorption isotherms of dr-MGC21 and dr-MG21 hybrid papers. The inset shows the corresponding pore size distribution of dr-MGC21 hybrid paper.

Fig. S8 XRD patterns of dr-MGC12, dr-MGC11 and dr-MGC21 hybrid papers.

Fig. S9 (a) XPS survey spectrum and (b) high resolution C 1s spectrum of GO/CNT hybrids.

Fig. S10 First three cycles of CV curves of dr-MoS_2 NSs measured in the voltage

range from 0.01 to 3.0 V at a scan rate of 0.1 mV s^{-1}.

Fig. S11 Comparison of the cycling performance of dr-MoS_2 NSs, df-MoS_2 NSs and bulk MoS_2 in the voltage range from 0.01 to 3.0 V at a current density of 0.1 A g^{-1}.

Fig. S12 Cross-sectional FESEM images of dr-MGC21 hybrid paper after the cycling process at (a) low and (b) high magnifications. The inset of (a) shows that the average thickness of dr-MGC21 hybrid paper after the cycling process is still about 8 μm.

Fig. S13 Comparison of the cycling performance of dr-MGC21 and dr-MG21 hybrid papers in the voltage range from 0.01 to 3.0 V at a current density of 0.1 A g^{-1}.

Fig. S14 Nyquist plots of dr-MGC21 and dr-MG21 hybrid papers measured in the frequency range from 100 kHz to 0.01 Hz with an AC voltage amplitude of 5.0 mV.

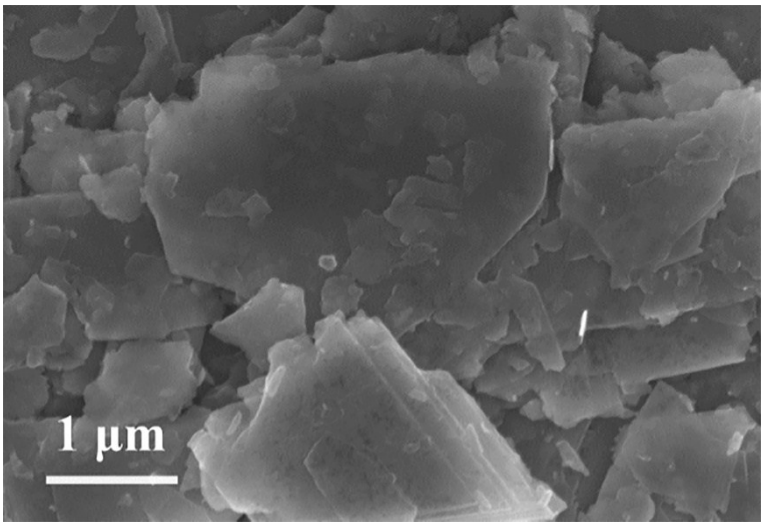

Fig. S1

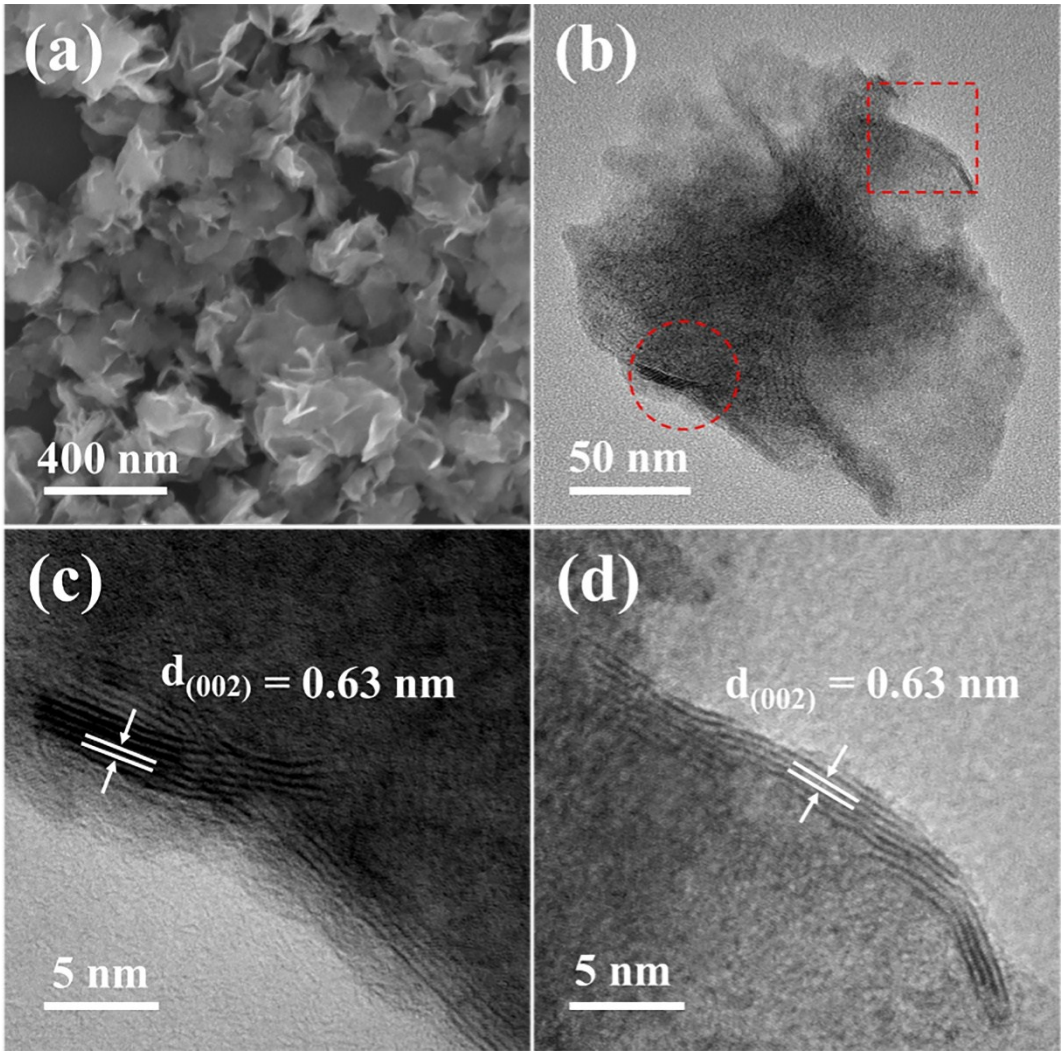

Fig. S2

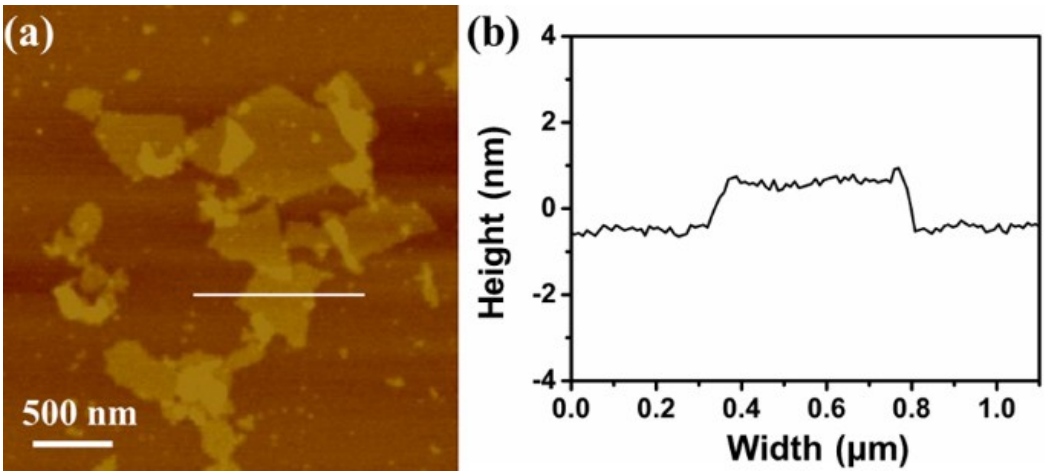

Fig. S3

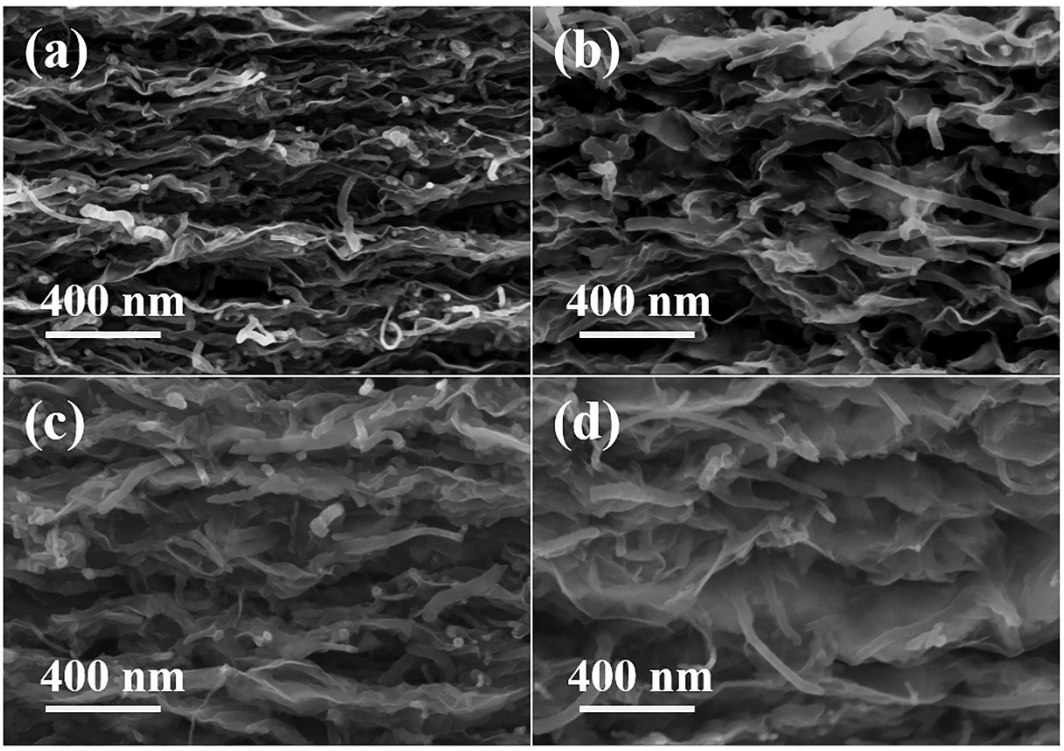

Fig. S4

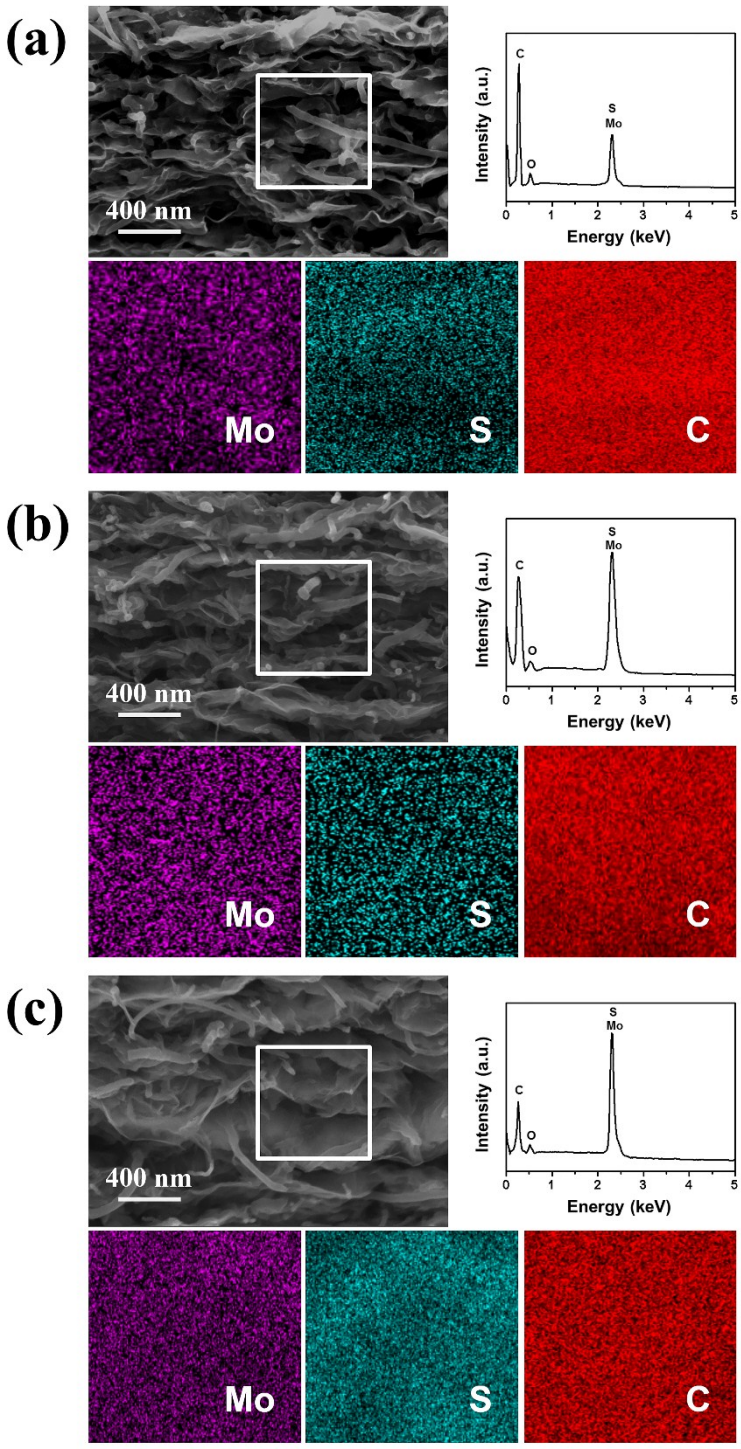
(a)
400 nm
C
S
Mo
O
Intensity (a.u.)
Energy (keV)
Mo
S
C
(b)
400 nm
C
S
Mo
O
Intensity (a.u.)
Energy (keV)
Mo
S
C
(c)
400 nm
C
S
Mo
O
Intensity (a.u.)
Energy (keV)
Mo
S
C

Fig. S5

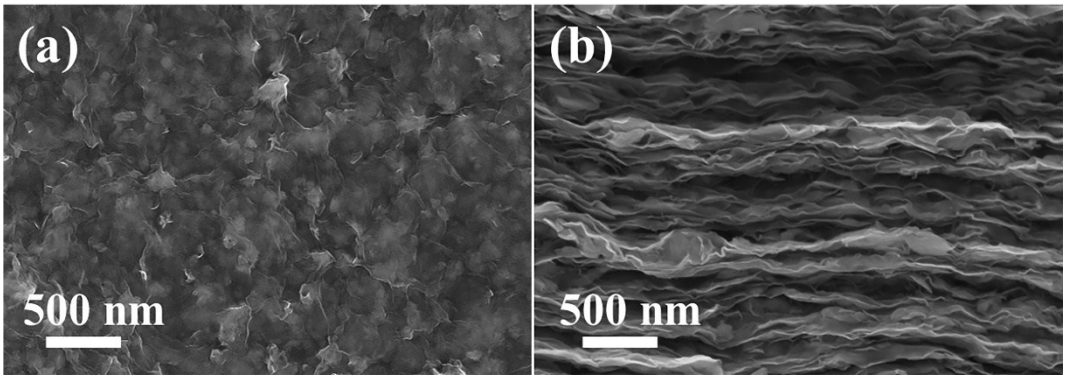

Fig. S6

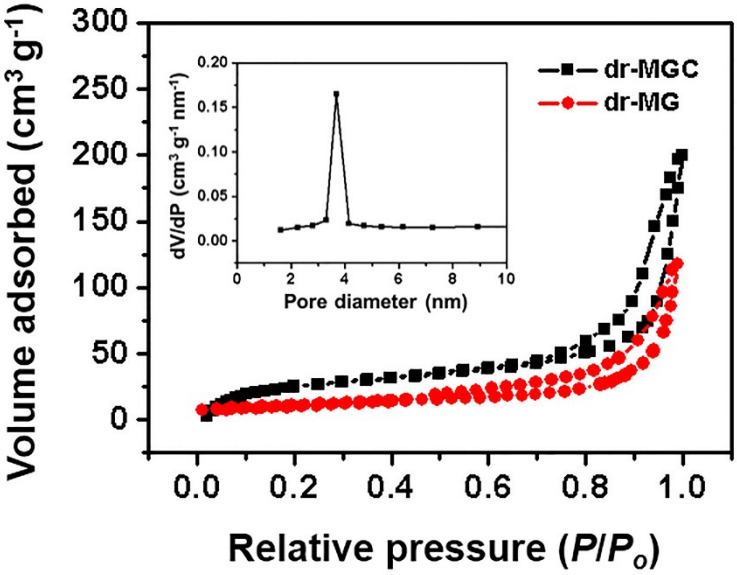
Volume adsorbed (cm^3 g^{-1})
300
250
200
150
100
50
0
0.0
0.2
0.4
0.6
0.8
1.0
Relative pressure (P/P_o)
dr-MGC
dr-MG
dV/dP (cm^3 g^{-1} nm^{-1})
0.20
0.15
0.10
0.05
0.00
0
2
4
6
8
10
Pore diameter (nm)

Fig. S7

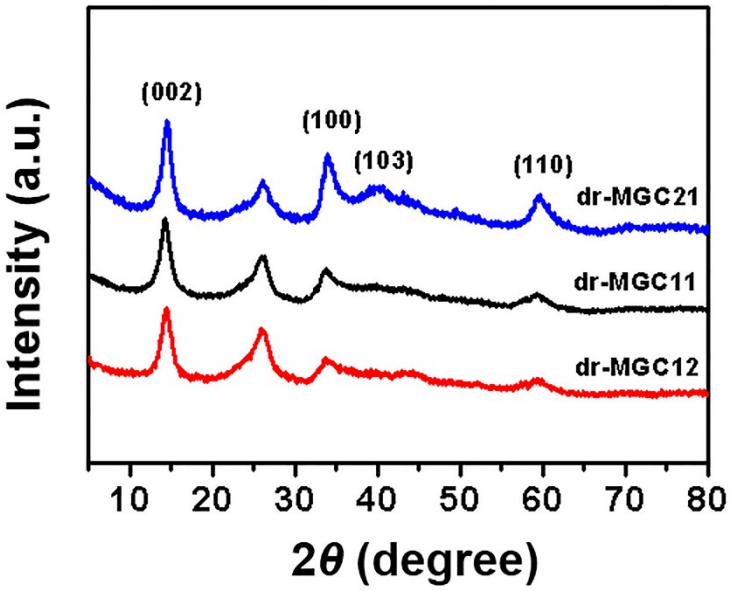
(002)
(100)
(103)
(110)
dr-MGC21
dr-MGC11
dr-MGC12
Intensity (a.u.)
10
20
30
40
50
60
70
80
2θ (degree)

Fig. S8

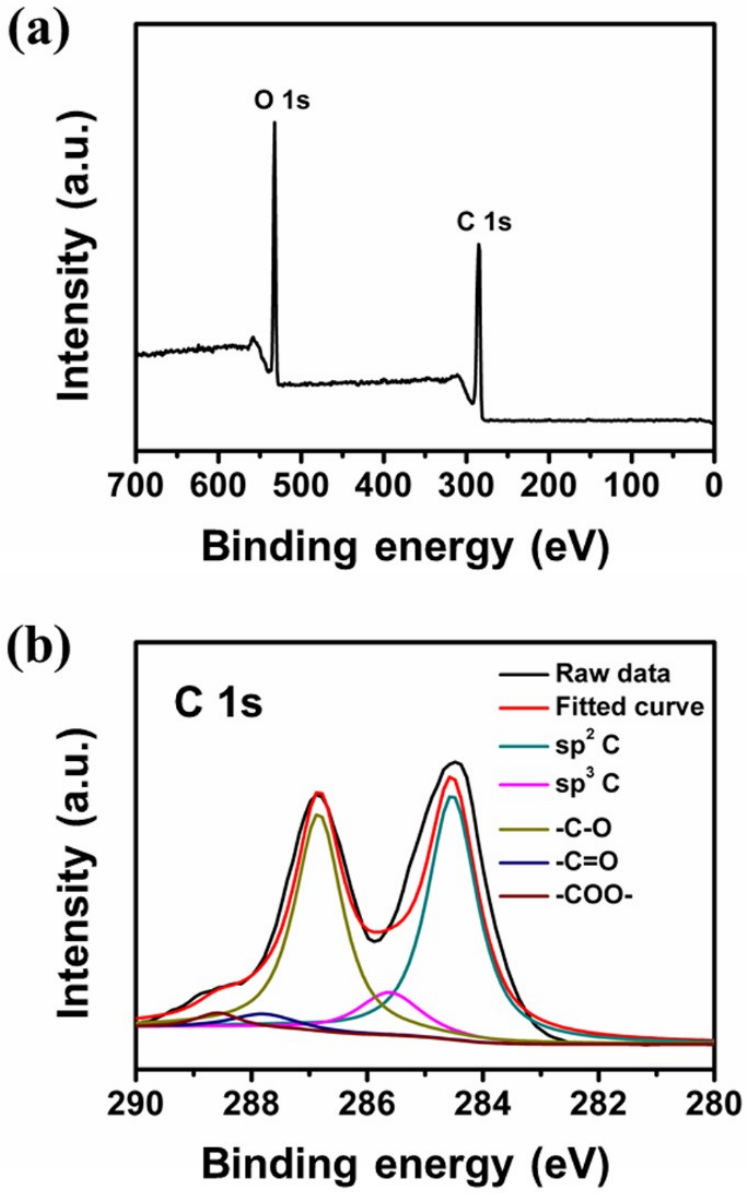
(a)
O 1s
C 1s
Intensity (a.u.)
700 600 500 400 300 200 100 0
Binding energy (eV)
(b)
C 1s
Raw data
Fitted curve
sp2 C
sp3 C
-C-O
-C=O
-COO-
Intensity (a.u.)
290 288 286 284 282 280
Binding energy (eV)

Fig. S9

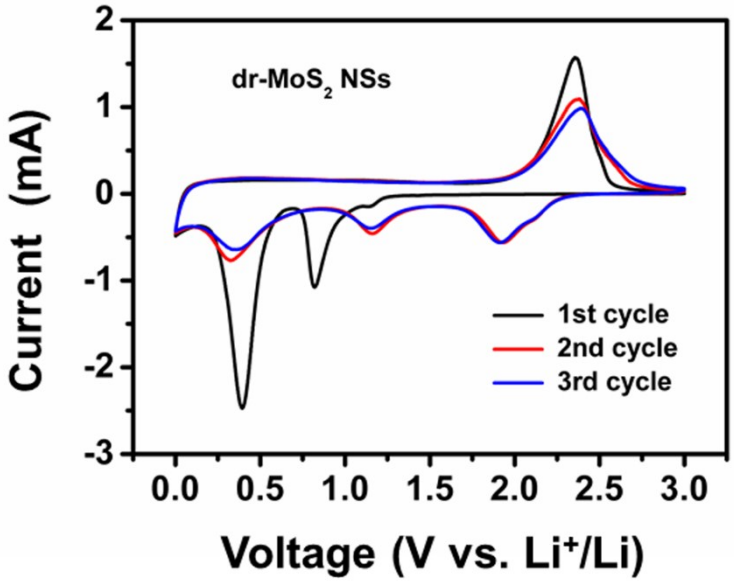
dr-MoS2 NSs
1st cycle
2nd cycle
3rd cycle
Current (mA)
Voltage (V vs. Li+/Li)
2
1
0
-1
-2
-3
0.0
0.5
1.0
1.5
2.0
2.5
3.0

Fig. S10

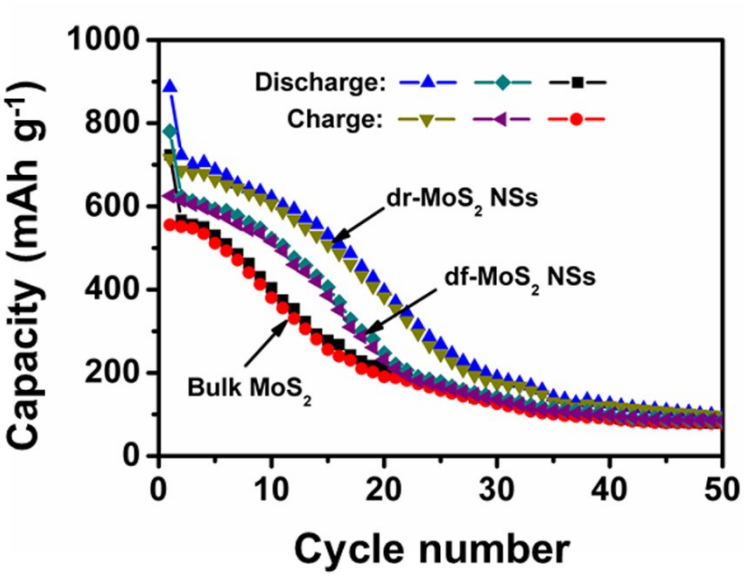
Capacity (mAh g-1)
Cycle number
Discharge:
Charge:
dr-MoS2 NSs
df-MoS2 NSs
Bulk MoS2
0
200
400
600
800
1000
0
10
20
30
40
50

Fig. S11

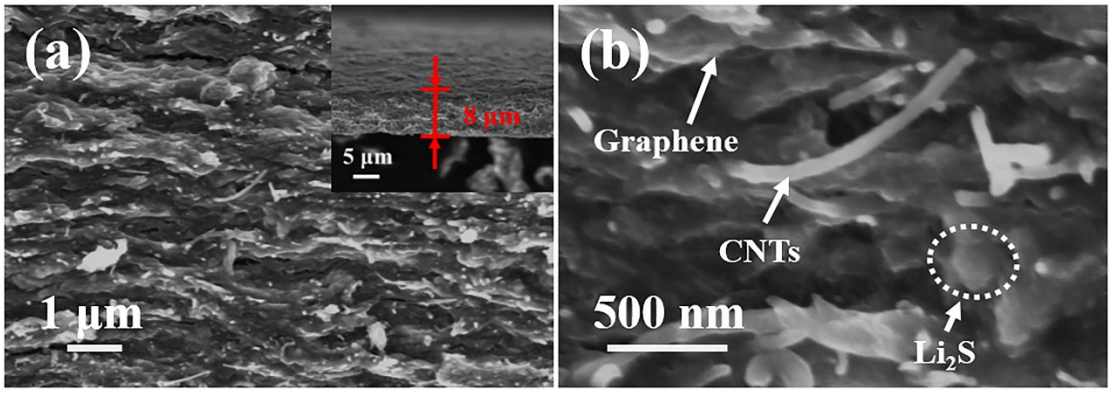

Fig. S12

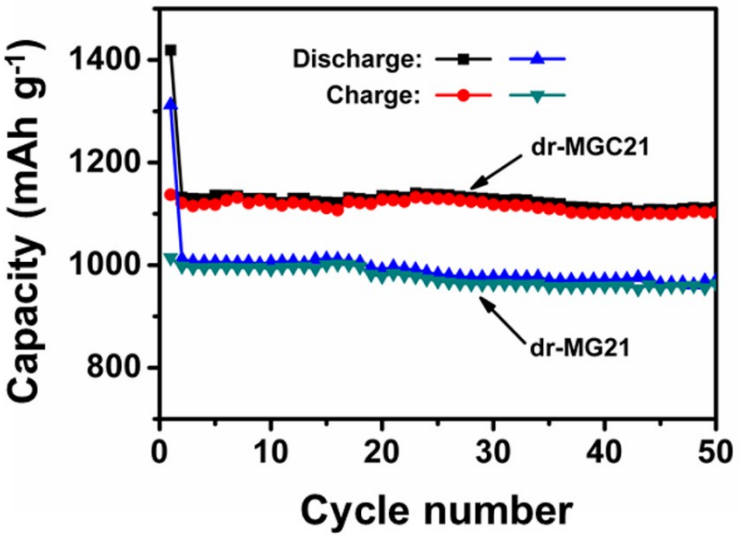
Capacity (mAh g-1)
1400
1200
1000
800
0
10
20
30
40
50
Cycle number
Discharge:
Charge:
dr-MGC21
dr-MG21

Fig. S13

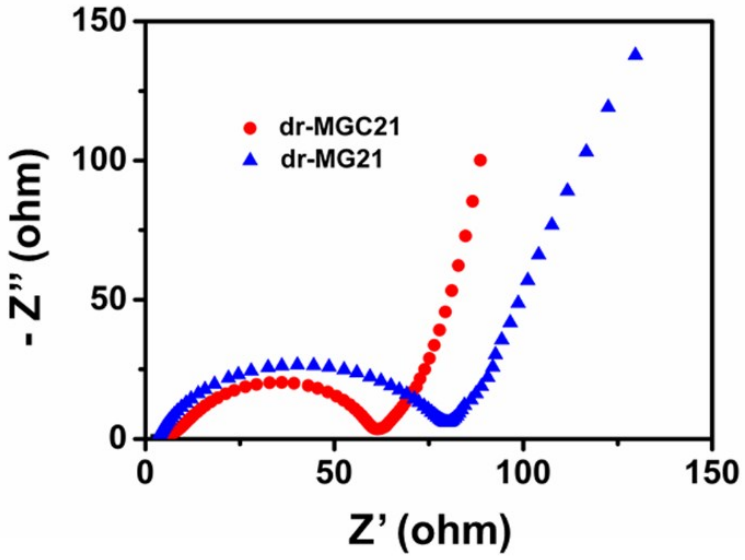

Fig. S14